Key Engineering Materials
ISSN: 1662-9795, Vol. 1050, pp 235-247
doi:10.4028/p-SA56ki

Submitted: 2026-01-21
Revised: 2026-02-16
Accepted: 2026-02-17
Online: 2026-04-16

Combined Experimental and Simulation-Based Approach for Optimizing Roll Forming of Pipes for Hydrogen Infrastructure

Murli Manohar Pandey[1,a*], Anja Rautenstrauch[1,b*], Andreas Kunke[1,c] and Till Clausmeyer[1,d]

[1]Professorship Forming Technology, Institute for Machine Tools and Production Processes, Chemnitz University of Technology, Reichenhainer Straße 70, 09126 Chemnitz, Germany

[a]murli-manohar.pandey@mb.tu-chemnitz.de, [b]anja.rautenstrauch@mb.tu-chemnitz.de, [c]andreas.kunke@mb.tu-chemnitz.de, [d]till.clausmeyer@mb.tu-chemnitz.de

Keywords: roll forming, modeling, FEM simulation, pipe.

Abstract. Roll forming pipes for hydrogen infrastructure poses particular challenges for process design, especially with regard to geometric accuracy and the avoidance of forming defects that could compromise the integrity of the pipelines. Geometric accuracy is crucial to ensure uniform pressure distribution within the pipe. Conventional trial-and-error approaches to developing roll flower designs are time-consuming and cost-intensive, especially when working with high-strength steel grades. This work presents an integrated methodology for roll forming of monolithic sheet by incorporating real-world machine stiffness and experimental anisotropy. A finite element model was developed for S235 and S355 steels, validated through three-point bending and Digital Image Correlation (DIC). While database-derived models (JMatPro) underestimated yield stress by up to 30%, the experimental model precisely predicted strain distribution trends with high precision, with local deviations remaining below 0.02 absolute strain. A central novelty is the integration of in-situ 3D laser scans of the roll forming mill under load, allowing the simulation to account for elastic machine deflections of up to 0.9 mm. The resulting simulation framework enables the accurate prediction of pipe geometry and process-induced residual stresses, which are critical for the long-term integrity of pipelines against hydrogen-induced cracking.

Introduction.

Roll forming is a key manufacturing process for pipeline tubes in energy infrastructure. In hydrogen applications, the process must satisfy especially high demands for leak tightness, material integrity, and geometric accuracy, since hydrogen can alter mechanical properties and increase susceptibility to hydrogen-induced cracking. Bolobov et al. show that compressed hydrogen affects the mechanical properties of pipeline steels [1], while Jia et al. and the BAM project report emphasize hydrogen-induced cracking and the sensitivity of welded microstructures to hydrogen exposure [2, 3]. Consequently, process-induced stresses and strain distributions must be controlled to ensure long-term pipeline safety.

Numerical simulation has therefore become increasingly important for roll forming process design. Egger et al. demonstrate the effective use of FE simulation for tube manufacturing including roll forming and welding [4], and Song et al. show that complex material behavior in high-strength steels can be captured by modern FE models [5]. Dong et al. further highlights the need for experimental validation in bimetallic pipe forming simulations [6]. However, many studies still rely on simplified or database-based material models, which are often not validated for the bending-dominated strain paths of roll forming. Yu et al. point out that supplementing material data and verifying simulations experimentally improves prediction accuracy [7].

Another challenge is the influence of machine and tool stiffness. Lamprecht et al. show that mill compliance significantly affects forming results and requires parameter identification [8], while the article from voestalpine highlights the importance of realistic process parameters for reliable FE simulations [9]. Validation in literature is often limited to final geometry or single process variables, as shown by Sheu and Jian in ERW tube simulations [10]. Studies on complex profiles and high-strength materials from Mahajan et al., and Suckow et al. underline the potential of FE simulation,

but a comprehensive coupling of experimental material characterization and process validation is still rarely established [11, 12].

Nevertheless, there is a challenge in appropriately considering the machine tool elasticity in simulations as well as process design. Moreover, the 'loaded' roll gap representing the active deformation state with the sheet inserted, deviates significantly from the theoretical tool geometry. While many studies assume an 'infinitely rigid' toolset, this simplification often yields geometric inaccuracies in the final product. This work addresses this limitation through an integrated methodology combining Finite Element Analysis (FEA) with real-world geometric deviations captured via portable 3D scanning. By quantifying the differential between unloaded and loaded machine states, a stiffness-compensated simulation model is proposed. This approach is essential for optimizing hydrogen-ready pipe forming, where even sub-millimeter geometric deviations can induce localized stress concentrations and premature failure.

Two complementary strategies were employed to derive the flow curves of material model. Initially, synthetic flow curves and mechanical properties were generated using JMatPro. Subsequently, these were compared against experimental data obtained via uniaxial tensile testing. The validity of the material models was assessed using three-point bending tests, where simulation results, specifically bending forces, profiles, and strain distributions, were compared against experimental measurements to evaluate predictive accuracy in bending-dominated forming processes.

The resulting comprehensive simulation framework enables the accurate prediction of global pipe geometry, cross-sectional strain distributions, and springback behavior. Furthermore, it identifies critical zones for potential edge waves and stress concentrations. The comparison between JMatPro-based and experimentally derived models quantifies discrepancies in plastic flow behavior and their subsequent impact on geometric accuracy. Ultimately, this close coupling of experiment and simulation explicates deformation mechanisms and significantly reduces the reliance on physical prototyping.

Material modeling

Accurate representation of JMatPro-based material behavior is crucial for simulating the roll forming process. In the approach, the material model for pipe steels such as S235 and S355 was developed taking into account the alloy composition and mechanical properties obtained from standardized tests. The materials to be investigated are the steel alloys presented in Table 1.

Table 1. Alloy composition of test material.

Material	Alloy composition [%]	Standard
S235	Al: 0.0021; Cr: 0.17; Cu: 0.35; Mn: 0.6; Mo: 0.02; Nb: 0.001; Ni: 0.11; Si: 0.21; Ti: 0.0011; V: 0.004; C: 0.07; N: 0.0057; P: 0.026; S: 0.035	DIN EN 10025-2
S355	Al: 0.0025; Cr: 0.06; Cu: 0.2; Mn: 1.09; Mo: 0.017; Nb: 0.002; Ni: 0.09; Si: 0.2; Ti: 0.002; V: 0.002; C: 0.18; N: 0.0082; P: 0.015; S: 0.012	DIN EN 10025-2

Table 2. Mechanical properties from tensile test.

Material	E [GPa]	$R_{p0,2}$ [MPa]	R_m [MPa]	A [%]	A_g [%]
S235	244.12	291.5	417.64	34.48	17.73
S355	240.64	393.5	485.27	28.18	13.98

Tensile tests were carried out in accordance with DIN 50125 to determine the yield strength and strength properties. The mechanical parameters elastic modulus E, yield strength $R_{p0,2}$, tensile

strength R_m, elongation at break A, and plastic uniform elongation A_g for 2 mm thick samples were derived from the test results and are presented in Table 2. The Ludwik relationship was used in this work to mathematically extrapolate the flow curves obtained from physical tests beyond necking region, for higher strains. It is a proven empirical model for mapping the hardening of metallic materials and describes the plastic flow behavior via the relationship as shown in Eq. 1.

$$k_f = k_{f0} + C * \varphi^n. \tag{1}$$

Here k_f is the true yield stress, k_{f0} is the initial yield stress, φ is the true plastic strain, C is the strength coefficient, and n is the work hardening exponent. The parameters C and n are determined to be 414 MPa and 0.406 for S235 material and 404 MPa and 0.430 for S355 material respectively, by regression analysis from the test data. The resulting flow curves are shown in Fig. 1.

The experimentally obtained flow curves exhibit generally larger stresses than the JMatPro-generated data. For S235, the experimental flow curve starts at approximately 300 MPa, whereas the JMatPro-based curve begins at around 210 MPa. A similar deviation is observed for S355, where the experimental flow curve starts at about 395 MPa, compared to 360 MPa from JMatPro.

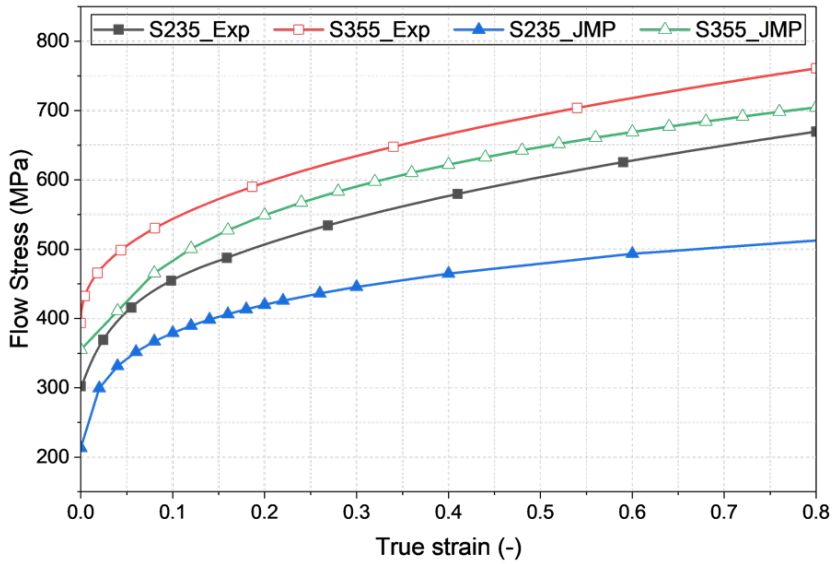

Fig. 1. Material flow curves derived and employed in Simufact forming.

These differences indicate an underestimation of the yield stress when using database-based material models and may lead to deviations in simulation results, particularly with respect to forming forces, stress and strain distribution, and springback. Therefore, the use of experimentally determined flow curves is beneficial for achieving more realistic process simulations.

To characterize the directional dependence of the material, tensile tests were performed on samples at 0° (rolling direction), 45° and 90°. A key parameter is the Lankford coefficient r, which describes the ratio of transverse strain to thickness change and is derived from the longitudinal and transverse strains measured during the tensile test.

$$r = \frac{ln(b_1/b_0)}{ln(s_1/s_0)}. \tag{2}$$

The Lankford coefficient r of the different orientations is used to calculate the mean anisotropy r_m and the planar anisotropy r_{plan}, which describe the average forming behavior and directional deviations.

$$\mathrm{r_m} = \frac{\mathrm{r_{0°}+2r_{45°}+r_{90°}}}{4}. \tag{3}$$

$$\mathrm{r_{plan}} = \frac{\mathrm{r_{0°}-2r_{45°}+r_{90°}}}{2}. \tag{4}$$

These characteristic values, as shown in Table 3, are crucial for the numerical simulation of sheet metal forming processes, as they supplement the material model with regard to the directional dependence of plastic flow and deformation properties.

Table 3. Material Anisotropy.

Material	Rolling direction [°]	Lankford coefficient r	Mean anisotropy r_m	Plane anisotropy r_{plan}
S235	0	0.370	0.391	-0.039
	45	0.410		
	90	0.374		
S355	0	0.495	0.535	-0.004
	45	0.539		
	90	0.568		

Validation of the material model

To validate the material model, three-point bending tests were performed in accordance with DIN EN ISO 7438 on a universal testing machine from Hegewald & Peschke (150 kN maximum force). The aim of the tests was to experimentally determine the maximum bending force, the resulting strains, and the resulting bending angle, and then to compare these values with the simulation results from Simufact Forming. This comparison made it possible to verify whether the material model correctly represents the real mechanical behavior of the steels under bending-dominated loading. Since, roll-forming is mainly dominated by bending operation, this serves as first validation.

The non-contact optical 3D measurement system ARAMIS Adjustable 24M was used for the precise recording of the shape changes during the bending tests. The system is based on digital image correlation (DIC) and point and pattern tracking of the sample surface (Fig. 2). To prepare the sample surface, a stochastic, high-contrast speckle pattern was applied, which the ZEISS CORRELATE software requires in order to precisely track displacements and strains. The pattern makes it possible to locate specific points on the surface in successive images and calculate their 3D coordinate changes.

During the tests, the system tracks surface changes in real time, allowing local strains, the bending angle, and geometric deviations caused by the process to be determined with precision. The data was then evaluated in ZEISS CORRELATE, yielding precise and reproducible results for the validation of the material models.

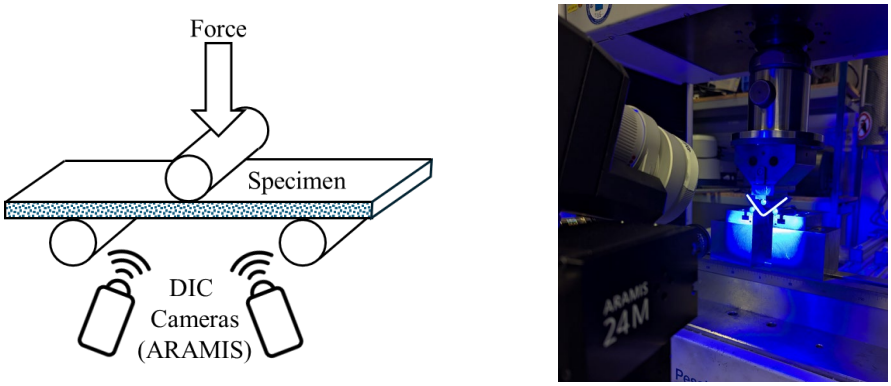

Fig. 1. Test setup Three-point bending tests according to DIN EN ISO 7438.

The experimental and numerical results show consistent trends in bending angle and force development for both S235 and S355 steels shown in Table. 4, where tensile test-based flow curves were used in the bending simulation. While the quantitative deviations in maximum force, specifically

the overestimation for S355, point to the limits of hardening parameters under pure bending, the consistent trends in bending angle and strain distribution confirm the model's overall reliability. Hill48 model was used for the yield criterion with Lankford coefficients (Table 3) as input parameters.

Table 4. Bending test – comparison of simulation vs. experiment.

Parameters			Experiment		Simulation	
Material	Rolling direction [°]	Feed motion of the bending punch [mm]	Bending angle [°]	Max. bending force [N]	Bending angle [°]	Max. bending force [N]
S235	0	4	20.5	1151	24.27	931
	0	8	45.5	1235	51.60	1135
	0	12	69	1155	73.83	1101
	0	16	87	1104	93.72	1101
	45	16	88.5	1225	93.72	1101
	90	16	88	1196	93.65	1101
S355	0	4	20	1167	22.33	1417
	0	8	45	1235	45.27	1505
	0	12	68.5	1195	67.69	1258
	0	16	88	1177	87.34	1258
	45	16	88	1196	87.35	1256
	90	16	88	1189	87.34	1258

The precise prediction of strain (error < 2%) verifies that the material model, incorporating batch-specific experimental flow curves and Hill48 anisotropy, effectively reflects the mechanical behavior required for the roll forming simulation. Fig. 3 shows the bending force–stroke curves obtained from the three-point bending tests. The experimental force curves for S235 and S355 show a significant overlap, with both materials reaching peak forces of approximately 1200 N. In contrast, the simulations reveal material-dependent deviations: the bending force for S355 is consistently overestimated, while the simulation for S235 underestimates the force during the initial stroke phase.

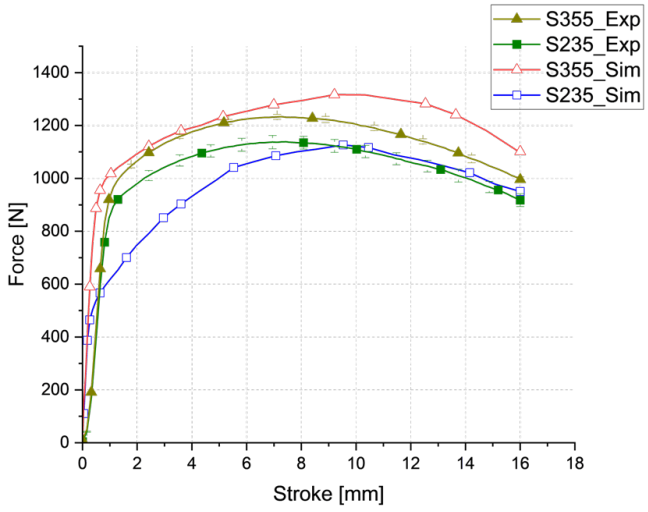

Fig. 2. Force-stroke curve in comparison simulation and experiment.

Fig. 4 depicts the strain distribution from experimental and numerical three-point bending tests for both investigated materials. For steel grade S235, a maximum strain of 0.2 was measured experimentally, while the simulation predicted a comparable value of 0.18, Similarly, for S355, the experimentally determined strain of 0.21 is closely matched by the simulated value of 0.23. The small deviations observed indicate that the material model is able to reliably reproduce the strain distribution under bending-dominated loading conditions. Overall, the results demonstrate that the simulation provides an accurate representation of the experimental behavior.

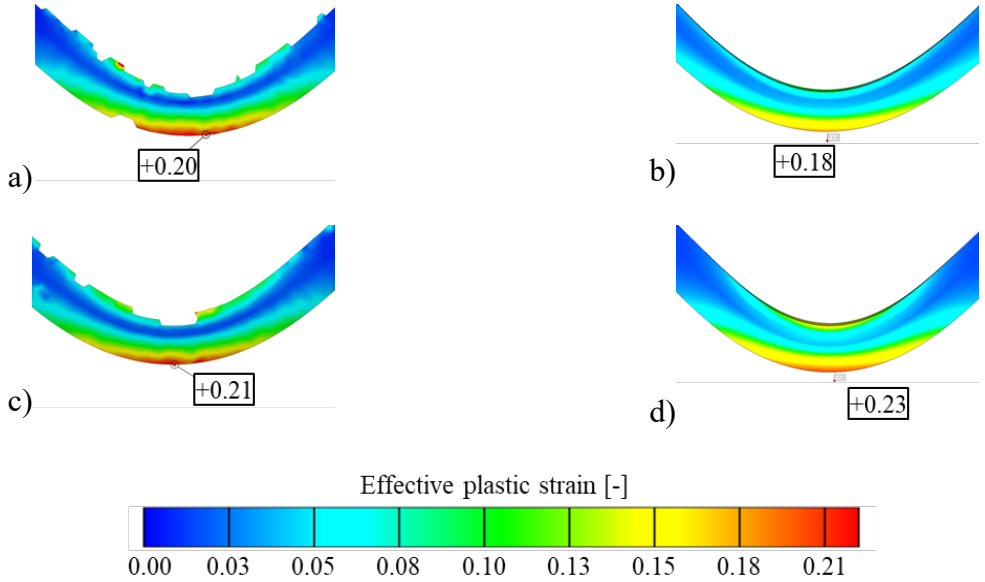

Fig. 3. Equiv. plastic strain distribution in bending test after springback– experiment vs. simulation (sample 90° to rolling direction) – a) S235 exp., b) S235 sim., c) S355 exp., d) S355 sim.

Comparison of material models

A detailed model was created in Simufact Forming 2025.2 for the numerical investigation of the roll forming process shown in Fig. 5.

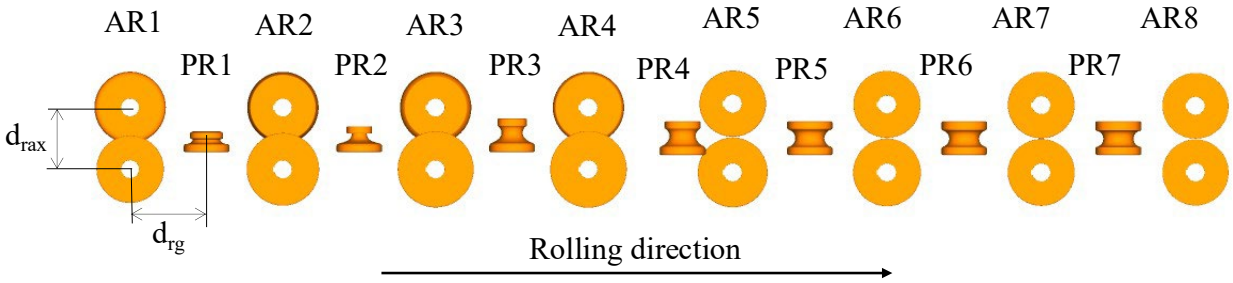

d_{rax} – roll center distance;
d_{rg} - roller gap

AR – active rollers;
PR – passive rollers

Fig. 4. Tool model.

The experimental validation was performed on a roll forming mill comprised of 15 stands arranged in a progressive flower design, utilizing 8 active (AR) and 7 passive (PR) roll stands. To bridge the gap between the theoretical design and production reality, the mill geometry was captured using a portable 'T-Scan hawk2' 3D scanner. This enabled in-situ measurement without machine disassembly, capturing roll profiles, positions, and alignments in the actual production environment. The measurement was performed in both unloaded and loaded states to capture process-induced elastic deflections due to forming forces. The geometric comparison of loaded state measurement to unloaded state is presented in Fig. 6. Deflection was determined by comparing loaded positions to unloaded baseline.

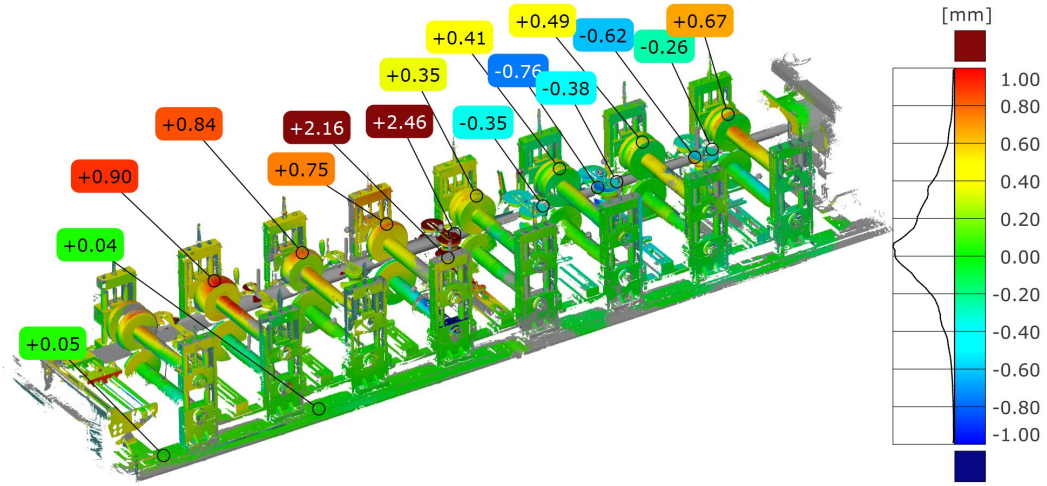

Fig. 5. Geometric deviation of the rolling mill in loaded state (with 2 mm sheet).

Along with the deflection evaluation, the axial position of individual roll as well as their relative distances to passive rolls were also evaluated. Maximum deviation of 2.5 mm was observed at passive stand 5, heavily containing positional error rather than elastic deflection. All the other stands were relatively stiffer, with approx. 0.9 mm maximum elastic deflection at roll stand 2 as shown in Fig. 6.

While many studies assume an 'infinitely rigid' toolset, leading to geometric errors, this model explicitly accounts for machine compliance. To maintain computational efficiency, the rollers are modeled as rigid bodies in Simufact Forming 2025.2, but their positions are adjusted to the measured 'loaded' roll gap identified during scanning. The numerical domain was discretized using solid hexahedral elements, with 5 physical layers across the 2 mm sheet thickness to capture through-thickness stress gradients. The blank geometry for the simulation was defined with dimensions of 800 mm in length, 183.78 mm in width. Furthermore, an inverse kinematic approach was adopted, where the sheet remains stationary while the forming stands translate; this method is mathematically equivalent to the physical process (6 m/min) and isolates geometric deformation from inertial effects. Although friction plays a minor role in roll forming simulation [13] and can be neglected, a Coulomb friction coefficient of 0.01 was applied to stabilize the model and isolate forming behavior. Table 5 summarizes the specific parameters employed in the roll forming simulation.

Table 5. Process definition for sheet roll forming (Mechanical model).

Simulation type	Implicit 3D
Ambient temperature °C	20
Workpiece starting temperature °C	20
Workpiece: Thermal transfer coefficient W/m²K	50
Tool starting temperature °C	20
Tool: Thermal transfer coefficient W/m²K	50
Process temperature	cold
Element type	Solid hexahedral
Feed rate mm/s	100

The aim of the simulation was to optimize the roll gaps and to compare material models, particularly the flow curves stored in JMatPro, with the experimentally determined material data from tensile test. The model enables the prediction of pipe geometry, strain distribution, and springback along the pipe length and across the width. By comparing the JMatPro-based simulation results with

the experimentally based material models, differences in plastic flow behavior and in the accuracy of the prediction for the pipe geometry can be quantified.

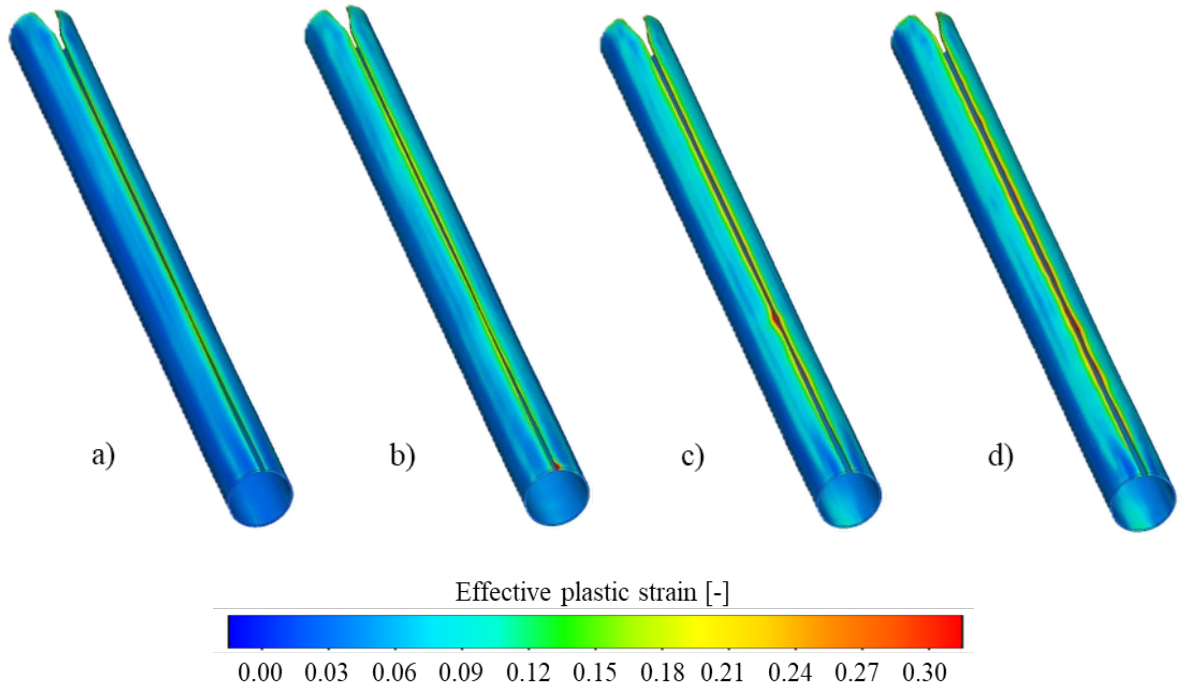

Fig. 6. Comparison of plastic strain simulated with material card JMatPro and experimental material data – a) S235 JMatPro. b) S235 exp. data. c) S355 JMatPro. d) S355 exp. Data.

Plastic strains from the simulations using the JMatPro material data were compared with those based on experimentally determined material data (see in Fig. 7). For both S355 and S235, the results show good agreement. Edge strains for S355 range from 0.21 to 0.30, while S235 exhibits edge strains between 0.13 and 0.18 in both simulation approaches. These findings confirm that the JMatPro-based material map reliably reproduces the experimentally observed plastic deformation and is suitable for predictive simulations.

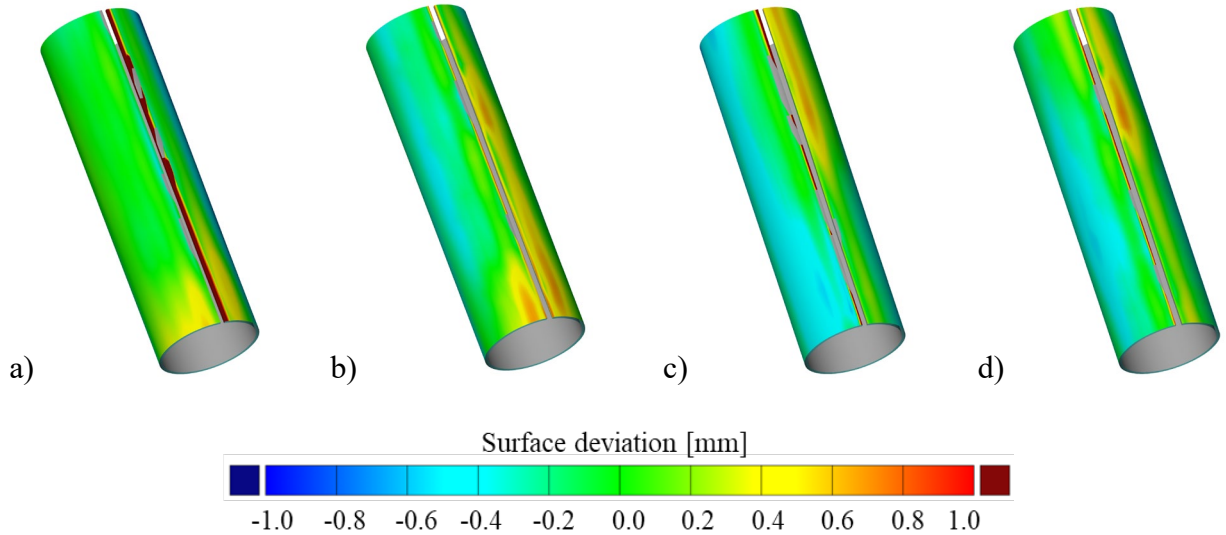

Fig. 7. Comparison of simulated pipe geometry with experimentally manufactured pipes – a) S235 JMatPro, b) S235 exp. data, c) S355 JMatPro, d) S355 exp. Data.

For consistency and to eliminate end effects, geometric comparison was performed on the mid sections of the manufactured pipes, utilizing the segment length of 220 mm to the simulated pipe geometry using both experimental and JMatPro-based material data (see in Fig. 8). For S235, surface deviations range from -0.2 to -0.4 mm, with edge deviations up to 1 mm. S355 shows similar deviations for both material maps.

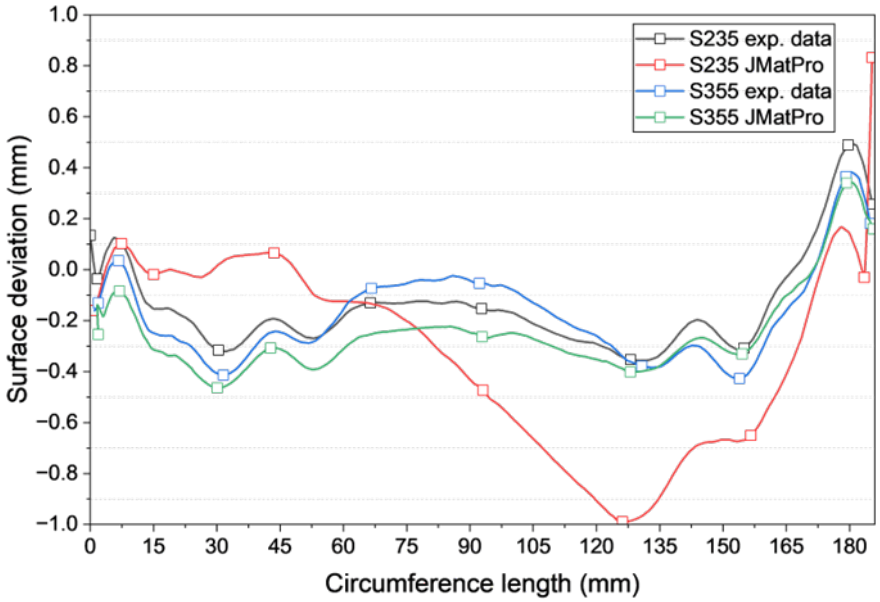

Fig. 8. Average surface deviation of simulated pipe segments (using different material models) from experimentally manufactured pipes (nominal).

Overall, both approaches reproduce the experimental pipe geometry well, with the largest discrepancies consistently occurring at the pipe edges. While deviations across the surface remain limited, S235JMatPro variant shows the largest deviation, reaching maximum deviation of 1 mm. The bow effect would explain the longitudinal deviations, while the asymmetric positioning of rolls in experiment might have caused the circumferential deviation. The simulation thus provides a basis for validating the material models in the context of pipe forming and shows the extent to which the theoretical flow curves from JMatPro reflect the actual behavior under the specific roll forming conditions as seen in Fig. 8 and Fig. 9.

Iterative Adjustment of Roll Gap for Realistic Simulation

The initial input data for the distance between the active top and bottom roller axes (d_{rax}) are based on the design concept used for roll tooling layout and serve as the reference for all subsequent iterations. The simulation was refined through a series of iterations to bridge the gap between design concept and production reality.

The design of the geometric parameters such as the distance of rollers in axial direction and selecting the roll gap depends on the target geometry of the profile and the material. Even smaller changes of the sheet thickness and the material grade or even the material batch require adaptations.

For this study. we refer to the initial state as "basic - design concept". Refinements of these settings for the roll gap are referred to as "1 - Real Data unloaded "i.e. the measured positions in the unloaded state, "2 - Real Data loaded "i.e. similar to 1, but with the sheet inserted, "3 - modified positions of stand 1 – 4" and "4 - modified positions of stand 5 – 8" refer to settings for subsequent simulations with adjusted geometric parameters. Therefore, 4 iterations of simulations were conducted. In the set-up of the simulations, one faces the challenge that using elastically deformable rollers is numerically too costly. However, applying rigid rollers with too small roll gaps, not accounting for the deformation in the experiments leads to contact problems and finally simulation terminations. As

discussed, “finding the nominal” and the “appropriate loaded” gap Is the main challenge discussed in this paper.

The roll gaps of AR1 to AR4 are dominated by the sheet thickness, while the roll gaps of AR5 to AR8 are dominated by end profile geometry. In Iteration 1 and 2, initial setting of real unloaded/loaded geometries resulted in simulation termination. This failure highlighted that the "as-built" machine state lacked the necessary roll gap to accommodate the 2 mm sheet thickness in the roll passes 1 to 4. Only after a targeted adjustment of roll passes 1 to 4 in Iteration 3, explicitly accounting for the 2 mm sheet thickness in the roll gap design, was it possible to achieve a stable and executable simulation of the roll forming process.

Table 6. Distance between active top and bottom roller axis d_{rax}.

Iteration / active roller	AR1	AR2	AR3	AR4	AR5	AR6	AR7	AR8
Basic - Design concept	242.0	242.0	242.0	242.0	269.0	266.0	263.6	261.0
1 - Real Data unloaded (±0.05 mm)	241.2	241.4	241.4	241.6	268.0	265.1	262.3	259.3
2 - Real Data loaded (±0.05 mm)	242.0	241.6	241.7	241.8	268.2	265.5	262.7	259.8
3 - Modified positions of stand 1 - 4	242.1	242.0	242.0	242.0	268.2	265.5	262.7	259.8
4 - Modified positions of stand 5 - 8	242.1	242.0	242.0	242.0	268.9	265.9	263.6	260.5

Upon completion of Iteration 3, the resulting profile was analyzed and found to exhibit torsional deformation as shown in Fig. 10. This observation provided the direct motivation for the asymmetric flow adjustments implemented in Iteration 4, which subsequently eliminated the torsion and improved the overall stability of the roll forming process, hence, a more balanced deformation sequence.

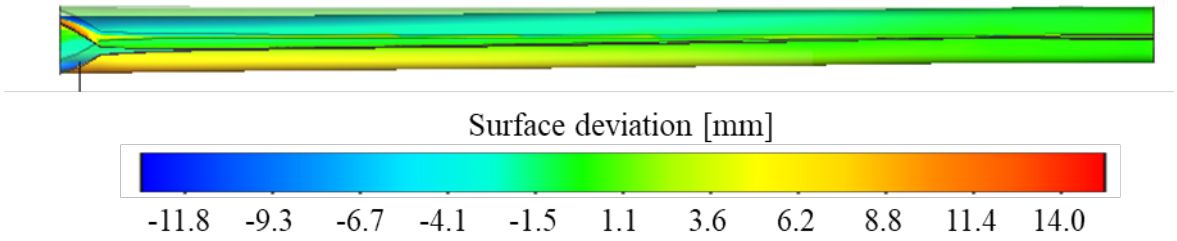

Fig. 9. Comparison of simulated pipe geometry from Iteration 3 (pre-optimization) to Iteration 4 (post-optimization)

Following the iteration 4, it was observed that the component did not exhibit torsion. A closer examination of the forming behavior in roll pass 8 revealed that while the profile in Iteration 3 maintained symmetrical contact with the rollers, it resulted in higher forming forces and residual torsion, as shown in Fig. 11.

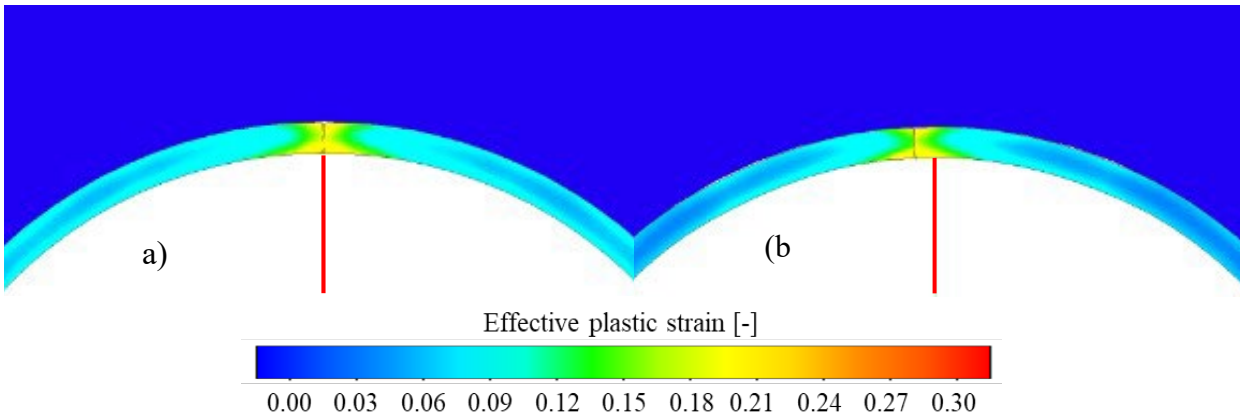

Fig. 10. Plastic strain of the formed pipes in the rolling gap 8 - a) Iteration 3 b) Iteration 4

In contrast to traditional design goals of perfect symmetry, Iteration 4 resulted in an asymmetrical deformation pattern in the pipe. Despite asymmetrical flow, this configuration required significantly less forming force while maintaining full contact of the pipe with the rollers. This indicates that the adjustments made in Iteration 4 altered the stress distribution and material flow, reducing the force demand in roll pass 8 while slightly changing the deformation pattern, as shown in Fig. 11 and Fig. 12.

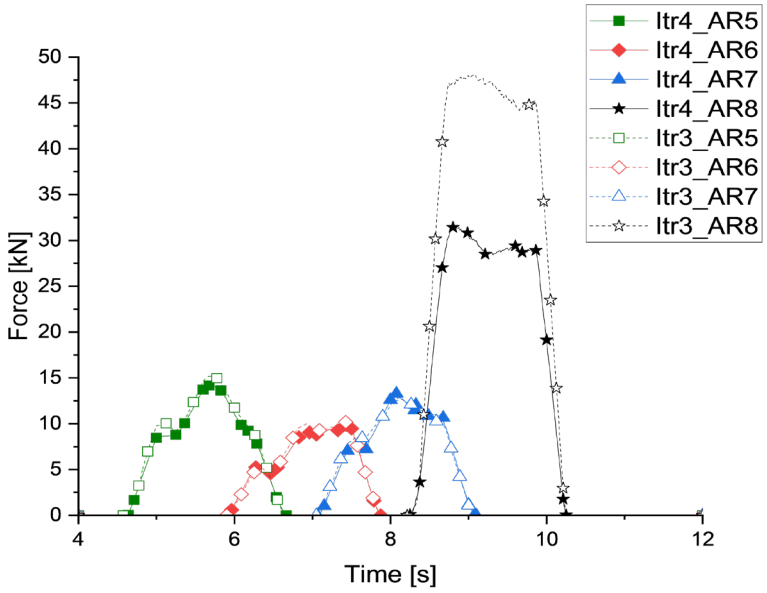

Fig. 11. Vertical forces in Roll forming stand AR5 to AR8 in Iteration 3 and 4

A more balanced stress state in the pipe is desirable because it prevents the formation of localized high-energy zones that can promote hydrogen accumulation and subsequent embrittlement. Consequently, the modified stress distribution achieved in Iteration 4 not only improves forming efficiency but may also reduce the risk of hydrogen-induced damage in the final component.

These findings highlight the importance of accurately capturing stress and material flow in the simulation model, since only a realistic representation of the forming process allows meaningful evaluation of design modifications. In general. the initial, more detailed examinations of the roller model indicate that the accuracy of the simulation closely reflects the component results when the models are adjusted as realistically as possible. Consequently, further investigations regarding the spacing and positions of active and passive rollers should be conducted to improve the predictive capability of the simulation.

Conclusion and Outlook

Roll forming of pipes is a key manufacturing process for hydrogen infrastructure and requires stringent safety, tightness, and dimensional accuracy. Conventional trial-and-error development is time-consuming and costly, particularly for high-strength steels. This study successfully established an integrated methodology that bridges the gap between theoretical tool design and the physical production environment. By incorporating batch-specific experimental anisotropy and loaded state machine deflection data, the predictive capability of the simulation was significantly enhanced, moving beyond the inaccuracies inherent in "infinitely rigid" tool assumptions.

Database-derived material models (JMatPro) were found to be insufficient for precise process design, as they underestimated the yield stress of S235 and S355 steels by up to 30%. In contrast, the experimentally derived Ludwik-based model accurately reflected the mechanical behavior in bending-dominated paths, predicting strain distribution with local deviations remaining below 0.02 absolute strain.

Portable 3D laser scanning identified process-induced elastic deflections of up to 0.9 mm in the rolling mill under load. The integration of these "loaded" gap measurements into the simulation framework proved essential for model stability; neglecting these deflections led to unrealistic contact problems and simulation terminations. A critical discovery in the final iteration 4 was that deviating from idealized symmetrical deformation patterns can be beneficial. Implementing a stiffness-compensated, asymmetrical flow successfully eliminated longitudinal torsion and significantly reduced the vertical forming forces required in the final roll passes.

The refined simulation provides a robust basis for controlling process-induced residual stresses. By achieving a more balanced stress distribution, the risk of localized high-energy zones, which are susceptible to hydrogen accumulation and subsequent hydrogen-induced cracking, is effectively minimized.

Building on this, future work will focus on systematically varying and optimizing the spacing and relative positioning of active and passive rolls. The goal is to better control material flow, minimize asymmetric stress states, and reduce geometric deviations at an early stage. This in-depth analysis can further enhance the predictive capability of the simulation and provide a robust basis for the optimal design of future roll forming processes.

Acknowledgment

The authors gratefully acknowledge the financial support provided by the Saxon State Ministry for Science. Culture and Tourism (Sächsisches Staatsministerium für Wissenschaft und Kunst. SMWK) through the CETPartnership program and EU funding under the research and innovation framework programs. This work was carried out within the framework of the project **HOOPLA** (Grant No. 100694930).

References

[1] V. I. Bolobov, Il'nur U. Latipov, G. G. Popov, G. V. Buslaev, Y. V. Martynenko, Estimation of the Influence of Compressed Hydrogen on the Mechanical Properties of Pipeline Steels, Energies 14(19) (2021) 6085. https://doi.org/10.3390/en14196085

[2] Y. Jia, H. Xue, Z. Wang, Research on hydrogen induced cracking behavior and service performance of metal pipeline material, Front. Mater. (2025). https://doi.org/10.3389/fmats.2025.1668151

[3] Federal Institute for Materials Research and Testing (BAM), Hydrogen-dependent mechanical properties of the welding microstructure of low-alloy steels for long-distance gas pipelines, BAM Project Report, Germany, 2023 2025. https://www.bam.de/Content/EN/Projects/hydrogen-dependent-mechanical-properties-steels/hydrogen-dependent-mechanical-properties.html

[4] C. Egger, M. Lüchinger, M. Schreiner, W. Tillmann, Numerical Simulation of Tube Manufacturing Consisting of Roll Forming and High Frequency Induction Welding, Materials 15(3) (2022) 1270. https://doi.org/10.3390/ma15031270

[5] J. Song. J. Lan. L. Zhu. Z. Jiang. Z. Zhang. C. Ma. Finite Element Simulation and Microstructural Analysis of Roll Forming for DP590 High Strength Dual Phase Steel Wheel Rims. Materials 17(15) (2024) 3795. https://doi.org/10.3390/ma17153795

[6] Z. Dong. Z, Xu. W, Wang. Z, Bi. J. Zhang, Numerical Simulation and Experimental Confirmation of a Bimetallic Pipe Forming Process, Materials 13(16) (2020) 3561. https://doi.org/10.3390/ma13163561

[7] Y. Yu, W. Haibo, L. Qiang, G. Yanzhi, Finite element simulation of flexible roll forming with supplemented material data and the experimental verification, Chin. J. Mech. Eng. 29 (2016) 1 12. https://doi.org/10.3901/CJME.2015.0824.106

[8] M. Lamprecht, E. Kocbay, M. Leonhartsberger, Y. Vetyukov, F. Bleicher, Nonlinear mechanical model of the shaft of a roll forming mill and parameter identification, Int. J. Adv. Manuf. Technol. 112 (2021) 3363 3375. https://doi.org/10.1007/s00170-020-06412-5

[9] voestalpine Roll Forming Corporation, Finite Element Analysis in Roll Forming Applications. ThomasNet Knowledge Center, 2022. https://www.thomasnet.com/knowledge/finite-element-analysis-in-roll-forming-applications/

[10] J.J. Sheu, E.-X. Jian, The ERW Tube Cold Roll Forming Simulation with Different Cage Roll Arrangement and Fin-Pass Design, Proceedings of the 14th International Conference on the Technology of Plasticity - Current Trends in the Technology of Plasticity. ICTP 2023. Lecture Notes in Mechanical Engineering. Springer. Cham. 2024. https://doi.org/10.1007/978-3-031-41023-9_35

[11] P. Mahajan, A. Abrass, P. Groche, FE simulation of roll forming of a complex profile with the aid of steady state properties, Steel Res. Int. 89 (2018) 1700350. https://doi.org/10.1002/srin.201700350

[12] T. Suckow, J. Schroeder, P. Groche, Roll forming of a high strength AA7075 aluminum tube, Prod. Eng. Res. Devel. 15 (2021) 573–586. https://doi.org/10.1007/s11740-021-01046-2

[13] Q.V. Bui, J.P. Ponthot, Numerical simulation of cold roll-forming processes, J. Mater. Process. Technol. 202 (2008) 275-282. https://doi.org/10.1016/j.jmatprotec.2007.08.073